Ionizing Radiation Effects in Silicon Photonics Modulators

Milana Lalović, Carmelo Scarcella, Anthony Bulling, Stéphane Detraz, Leonardo Marcon, Lauri Olanterä, Theoni Prousalidi, Ulrik Sandven, Christophe Sigaud, Csaba Soos, and Jan Troska

***Abstract*— Silicon photonics (SiPh) shows considerable potential as a radiation-hard technology for building the optical data transmission links for future high-energy physics (HEP) experiments at CERN. Optical modulators are a key component of optical links, which will need to withstand radiation doses in excess of 10 MGy. The geometrical parameters and doping concentrations of two popular types of SiPh modulators, Mach–Zehnder and ring modulators (RMs), have been varied in order to study their impact on the device radiation tolerance. They were exposed to an X-ray beam to test their resistance to ionizing radiation. The RM with the highest doping concentration is shown to be the most tolerant, showing no degradation in performance up to the highest dose of 11 MGy. Moreover, we report first evidence of the dependence of the radiation tolerance on the RM operating temperature.**

***Index Terms*— CERN, high-energy physics (HEP), ionizing radiation, Large Hadron Collider (LHC), Mach–Zehnder modulator (MZM), radiation effects, ring modulator (RM), silicon photonics (SiPh), total ionizing dose (TID), X-ray.**

I. Introduction

THE proton–proton collisions in the Large Hadron Collider (LHC) at CERN generate high levels of radiation in the measurement systems of the detectors that observe the collisions. In addition, these systems produce a vast amount of measured data. The planned high luminosity (HL-) upgrade of LHC is expected to increase the beam luminosity by five to seven times compared to present levels [1]. Higher luminosity generally leads to a greater number of collisions. Hence both the amount of data produced and the levels of radiation will increase significantly. Specifically, devices and components installed in the inner-most detectors of the HL-LHC will have to withstand a total ionizing dose (TID) greater than 10 MGy and a minimum 1 MeV-equivalent neutron fluence of more than 1.6×10^{16} n/cm^2. Traditional optical data transmission systems based on directly modulated lasers and photodiodes cannot sustain such high levels of radiation [2], and new systems and components must be identified in order to meet the challenge.

Silicon photonics (SiPh) is a technology currently being investigated that promises to sustain the estimated increases in both radiation level and data rate. This technology enables the combining of light-manipulating structures such as waveguides and couplers with doped regions of silicon to form p-n junctions that can manipulate light through the effect of the carrier concentration on refractive index. The SiPh production process is compatible with CMOS technology, opening the possibility of integration with electronic circuits that can potentially lead to the realization of low-mass and low-power components. The study of radiation effects in opto-electronic devices and systems is a rich and diverse field which brings together several challenges in both the measurement and understanding of the various effects. One of the major challenges is that, as their name suggests, opto-electronic devices combine effects in the electronic and optical domains. Thus, for a photonic integrated circuit one must be aware that static and transient effects might be induced in the waveguides themselves [3], [4], as well as in the active devices themselves [5]. The interested reader is invited to consult a recent review paper [6] for more details.

While it has previously been shown that SiPh Mach–Zehnder modulators (MZMs) can withstand TID levels up to a few hundred kGy [7], sufficient for a large number of potential terrestrial and space applications, new particle physics experiments are in preparation requiring tolerance to the much higher levels mentioned above. Based on the findings of [8] and the hardening by design (HBD) methods suggested therein, a new silicon photonics integrated circuit (PIC) with a novel and improved design of the SiPh modulators was designed at CERN and then fabricated by imec [9] as a part of a multi-project wafer (MPW) run. The radiation tolerance of the resulting PICs has been studied using an X-ray source and the results are reported below.

II. Devices Tested

A. SiPh Modulators Designs

The devices integrated on our most recent SiPh chip (PICv2) are based on a typical SiPh p-n junction phase shifter (see Fig. 1). When a reverse voltage is applied to the contacts, a phase shift of the light propagating through the waveguide is induced due to the plasma dispersion effect. Two kinds of

Manuscript received 15 December 2021; revised 17 January 2022; accepted 18 January 2022. Date of publication 1 February 2022; date of current version 18 July 2022.

Milana Lalović is with the School of Electrical Engineering, University of Belgrade, 11000 Belgrade, Serbia, and also with the EP-ESE Department, CERN, 1211 Geneva, Switzerland (e-mail: milana.lalovic@cern.ch).

Carmelo Scarcella, Anthony Bulling, Stéphane Detraz, Leonardo Marcon, Lauri Olanterä, Ulrik Sandven, Christophe Sigaud, Csaba Soos, and Jan Troska are with the EP-ESE Department, CERN, 1211 Geneva, Switzerland.

Theoni Prousalidi is with the School of Electrical and Computer Engineering, National Technical University of Athens, 157 80 Athens, Greece, and also with the EP-ESE Department, CERN, 1211 Geneva, Switzerland.

Color versions of one or more figures in this article are available at https://doi.org/10.1109/TNS.2022.3148579.

Digital Object Identifier 10.1109/TNS.2022.3148579

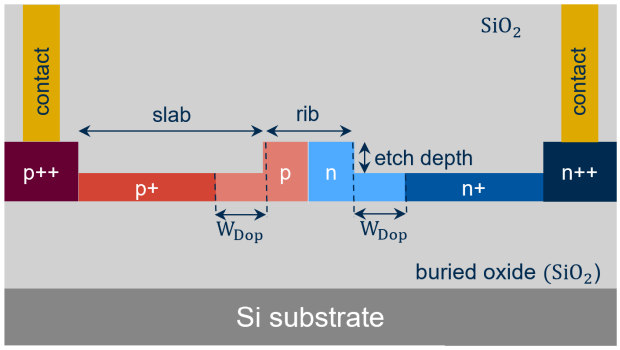

Fig. 1. Cross section of a typical SiPh phase shifter with lateral p-n junction. The tested devices have different rib widths, w_{Dop}, as well as doping concentrations.

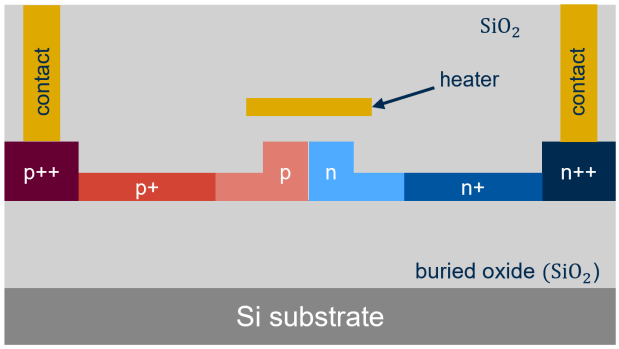

Fig. 2. Cross section of a typical SiPh phase shifter with a lateral p-n junction and tungsten micro-heater above the rib.

TABLE I
OVERVIEW OF THE DESIGN PARAMETERS OF THE TESTED DEVICES

	Device	w_{Dop} (nm)	Relative Doping Concentration	
			rib (p/n)	slab (p+/n+)
PICv1	MZM design a	300	3x	11x
	RM design b	100	5x	
PICv2	MZM design a'	300	1x	50x
	MZM design b'	100	1x	
	RM design b'	100	1x	
	RM design b''	100	10x	

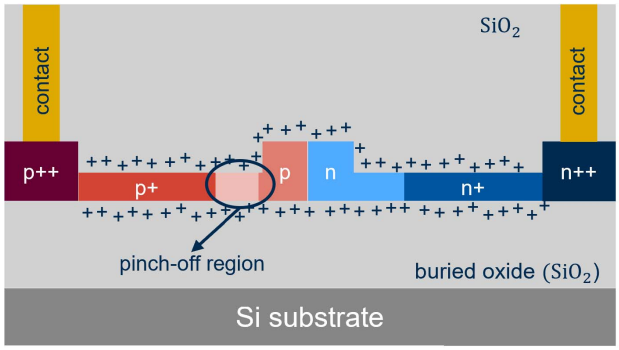

Fig. 3. Cross section of a typical SiPh phase shifter with lateral p-n junction. The fixed positive charge is generated at the interface Si/SiO_2 by high-energy particles. The pinch-off region is a consequence of ionizing radiation damage.

modulator design were included on PICv2: MZMs and ring modulators (RMs). The devices presented here have similar geometrical design parameters to those on our previous chip design (PICv1) [7]. One key difference between PICv1 and PICv2 is that the latter was manufactured in the improved fabrication process now available from the foundry. One of the major changes in the process is the change in nominal doping concentrations in the different cross section regions shown in Fig. 1. While the absolute values of these doping concentrations are not revealed by the foundry, the values normalized to the overall lowest doping concentration are reported in Table I.

All modulators have the same etch depth of 160 nm and rib height of 220 nm. The rib width in the case of MZMs is 450 nm and for RMs is 500 nm. The slab widths of MZMs and RMs are 1275 and 1000 nm, respectively. The values for the w_{Dop} were varied in order to achieve more radiation tolerance and are shown in Table I. We evaluated two different MZMs designs with $w_{\mathrm{Dop}} = 300$ and 100 nm, respectively. Moreover, we evaluated the radiation hardness of three RM implementations, all with the same w_{Dop}, and with rib and slab doping concentrations reported in Table I. The free spectral range (FSR) of RMs is 19.3 nm and for MZMs it is 18.4 nm.

B. RMs With Micro-Heaters

One important difference between MZM and RM designs is the micro-heater [10], [11] integrated on top of the RM waveguide. Heaters are popular solutions for fine-tuning phase shift thanks to simple operation and integration in the wafer fabrication process. The high thermo-optic coefficient of silicon makes SiPh devices very sensitive to temperature variations. Therefore, integrated micro-heaters are used to actively compensate for environment temperature changes and chip manufacturing tolerances (see Fig. 2). The heater is operated applying a voltage to its contacts. The resonance wavelength shifts linearly with temperature about 70 pm/°C, while the heater used in this work shows an efficiency of about 4 °C/mW.

III. IONIZING RADIATION EFFECTS IN SIPH

During exposure to ionizing irradiation, damage occurs when high-energy particles passing through the oxide generate a layer of fixed positive charge [12], [13] at the interface between Si and SiO_2. This fixed charge then interacts with free holes in the p-doped Si pushing them away until the concentration of free holes is so low that there is no conductive path between the p++ contact and the rib junction anymore. This effectively prevents the voltage-induced variation of the carrier concentrations in the waveguide making the phase-shifter inoperable. The part of p-doped Si with very low concentration of holes thus created is called the pinch-off region, as shown in Fig. 3.

Regarding the impact of the heater on the dose delivered to the p-n junction, after calculation based on the Beer–Lambert law using tungsten as material and 10 keV X-rays, the additional attenuation due to the heater is below 10%, therefore

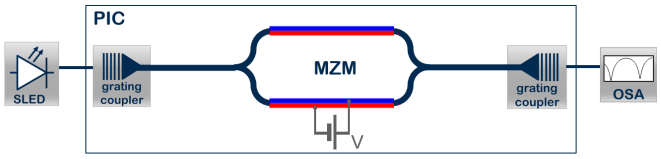

Fig. 4. Measurement setup for MZMs, with the reverse bias voltage V applied to one of the two arms.

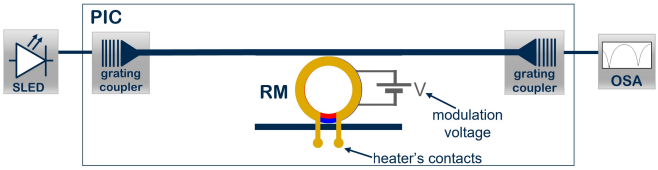

Fig. 5. Measurement setup for the RM, with the reverse bias voltage V applied to the ring p-n junction. A tungsten heater was fabricated above the ring waveguide.

negligible. The heater is 600 nm wide, and it covers the whole rib region and a small portion of the low doping slab. The rest of the slab is not covered by the heater, and the dose will be the same as in the case of structures without heater.

IV. Measurement Setup

The effects of ionizing radiation on the SiPh devices were measured using the X-ray irradiation facility at CERN [14], where a vacuum tube with a tungsten target produces X-rays with an energy spectrum peaking at 10 keV. The power supply voltage of the tube is 40 kV, and the current is 50 mA. The SiPh chip was exposed to more than 11 MGy(SiO_2) of TID at a dose rate of 15.83 Gy/s. The reference material for TID throughout the article is SiO_2. During the irradiation, the PIC substrate temperature was kept at 25 °C.

The measurement setup diagrams for MZMs and RMs are shown in Figs. 4 and 5, respectively. A superluminescent diode (SLED) with a central wavelength of 1550 nm was used as input broadband light source. The light coming from the SLED was coupled into the chip via grating couplers and the light was further guided through an integrated waveguide to the modulator. Another grating coupler was placed at the modulator output to couple the light back into an optical fiber connected to the optical spectrum analyzer (OSA) used to record the transmitted optical spectrum. An example of the transmission spectra of the RM for two different bias voltages is shown in Fig. 6, where the resonance wavelength is defined as the minimum of the spectrum. A shift in the resonance wavelength is induced by applying a reverse bias voltage to the modulator. The main performance parameter of RMs, the modulation efficiency, is defined as the resonance wavelength shift induced by 1 V of reverse bias change. Changes in modulation efficiency during irradiation, normalized to the pre-irradiation value, are shown in the following results.

In addition to the electro-optical effect, the thermo-optical effect can be used to induce resonance wavelength shift in RMs. Micro-heaters are used to locally set the temperature of the RM with the intent to characterize the radiation tolerance at different temperatures. The resonance wavelength shift induced by the temperature settings is not included in the modulation efficiency calculation, as it provides a constant offset regardless of the bias voltage.

In the following, all presented results for RMs are at 25 °C, unless otherwise stated. The transmission spectra of the modulators were measured sequentially using an optical switch. At the end of the test, the X-ray source was turned off, while the measurement loop continued for 150 h.

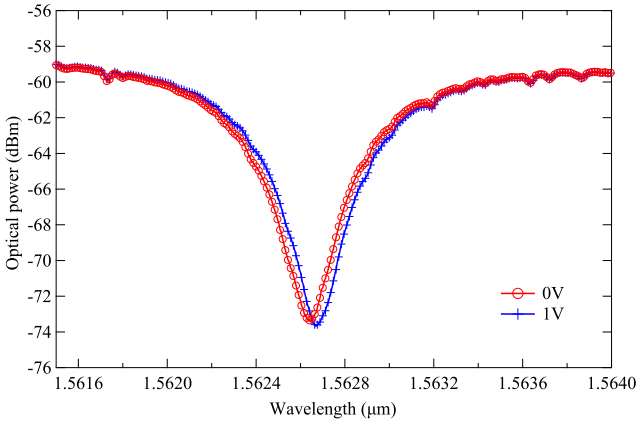

Fig. 6. Example of RM transmission spectra, at 0 and 1 V reverse-bias voltage.

V. Results and Discussion

All results presented are divided into three measurement stages: pre-irradiation, during irradiation, and post-irradiation (with the exception of post-irradiation data for PICv1). The pre-irradiation data for PICv1 is a single data point. During the test, the RMs were operated at 1 V reverse bias voltage on average, which is a good approximation of the average bias voltage applied to the modulators when integrated into a transmitter for data communication [15], [16]. All modulation efficiencies reported in the following are measured as the difference in resonance wavelengths when 0 and 1 V bias voltage is applied to the modulators.

A. Mach–Zehnder Modulators

Two different types of MZMs were tested, design *a* and design *b*, Table I. In Fig. 7, the radiation tolerance of the same MZM design on the two versions of the chip is compared. This gives an indication of the impact on radiation tolerance introduced by the foundry process changes. The normalized modulation efficiency as a function of TID for the MZM design *a* is plotted in Fig. 7. The measured modulation efficiency is approximately constant until a dose of 70 kGy(SiO_2) for design *a* and until a dose of 1 MGy(SiO_2) for design a', after which it quickly approaches zero. Since both devices have the same geometrical design parameters, the improvement in radiation-hardness is due to changes in the production process and differences in doping concentrations in the rib and slab regions. The lower doping concentration in the rib region lead to better optical performance of MZMs [17], while higher doping concentration in the slab region indicates more effective

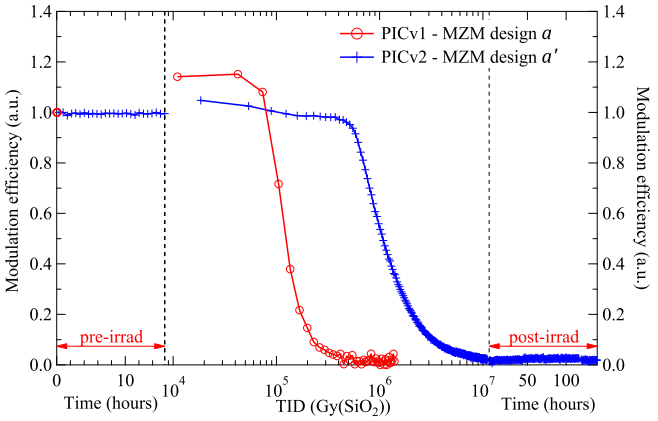

Fig. 7. Modulation efficiency degradation with TID of MZM design a normalized to its pre-irradiation value for the two PIC versions.

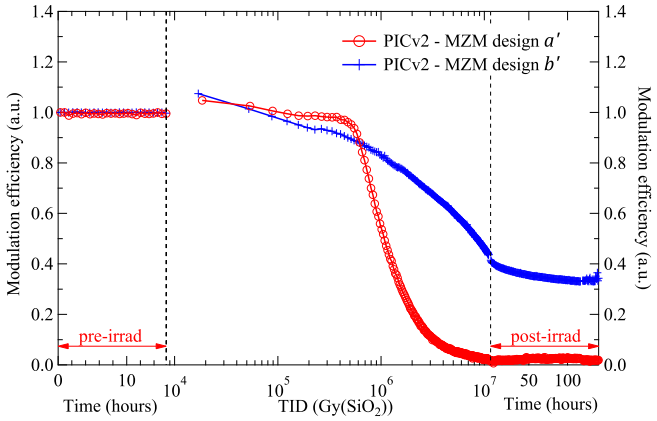

Fig. 8. Modulation efficiency of the MZM design a' and design b' normalized to its pre-irradiation value.

compensation for ionizing radiation damage in the pinch-off region. Note that the modulation efficiency of the MZM from PICv1 is greater than 1 at the beginning of the irradiation before it starts to degrade. This effect was previously reported in [5], [7], and [18]. A possible explanation is that when a fixed positive charge is deposited at the Si/SiO_2 interface, free carriers in the rib are pushed toward the center of the rib. This effect influences the effective refractive index of the waveguide and the phase shift. The induced phase shift results to be stronger for the same bias voltage, which reflects in an enhancement of the modulation efficiency.

In Fig. 8, the difference in the modulation efficiency degradation between the MZM design a' and design b' of PICv2 is shown. The MZM design a' started rapidly to degrade after 1 MGy(SiO_2). However, the MZM design b' degraded more slowly with the increase of TID. Remarkably, it is still operable after 11 MGy(SiO_2), but with reduced efficiency of 40% of its pre-irradiation value. The main difference between design a' and design b' is in the width of w_{Dop}, which is shorter in the latter case. By reducing w_{Dop}, the possible pinch-off region is shorter, and the p+ doped region will easily compensate the lower concentration of free holes. Hence, the radiation tolerance increases with the reduction of w_{Dop}.

B. Ring Modulators

RMs are far more compact and easier to integrate than the MZMs because of their small footprint. The radius of the RM is just 5 μm, while the lengths of the arms of the MZM are of the order of 1 mm. With that advantage, it was a logical choice to include them in these experiments.

The modulation efficiency of the PICv1 RM is represented by the red curve in Fig. 9. It begins to rise slowly until 200 kGy(SiO_2) and then rapidly starts to degrade, finally falling down to zero at 500 kGy(SiO_2). The blue curve in Fig. 9 shows the behavior of the same design of RM on PICv2 but with three times lower doping concentration. Although it was expected for RM with the lowest doping concentration to be the least radiation tolerant, the higher doping concentration

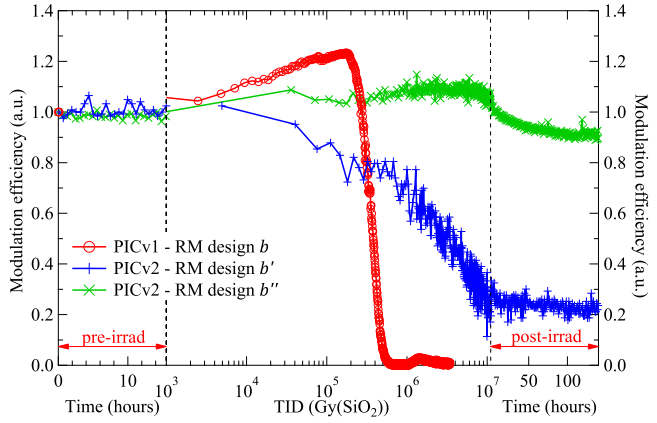

Fig. 9. Modulation efficiency of the three tested RM designs normalized to its pre-irradiation value for different doping concentrations.

in the slab region influenced RM design b' to be more radiation tolerant than RM design b. Even though this design is more radiation tolerant than the RM from PICv1, it still degrades and has almost no modulation efficiency after 11 MGy(SiO_2). The green curve shows the RM design with ten times higher doping concentration than nominal. Surprisingly, this design stays fully functional even after the TID of 11 MGy(SiO_2). Once the X-ray beam was turned off, the measurement of transmission characteristics was continued for the following 150 h with the goal of observing possible post-irradiation annealing. Whilst keeping the same measurement conditions during this time, only a gradual decrease of efficiency to 90% of its pre-irradiation value was noticed. This is possibly happening due to the leftover charge trapped at the Si/SiO_2 interface, which will diffuse further from the waveguide over time, thus the enhancement of the modulation efficiency will disappear. The significant difference between RM design b' and design b'' could be attributed only to a difference in the doping concentrations of the p-n region. This is consistent with previous work on MZMs showing that a higher doping concentration in the rib enhances radiation resistance [19].

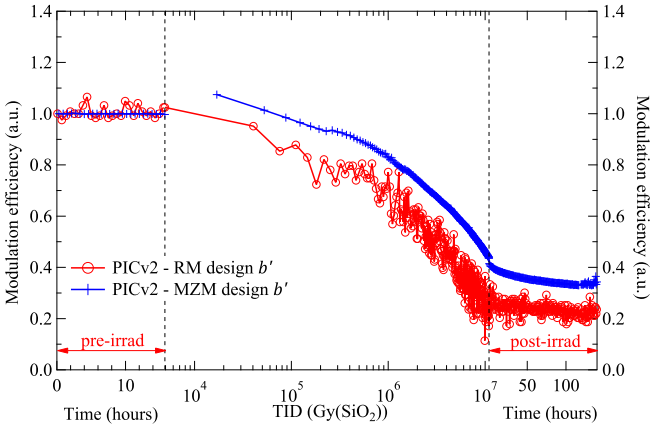

Fig. 10. Modulation efficiency of the design b' modulators of the PICv2 normalized to their pre-irradiation value.

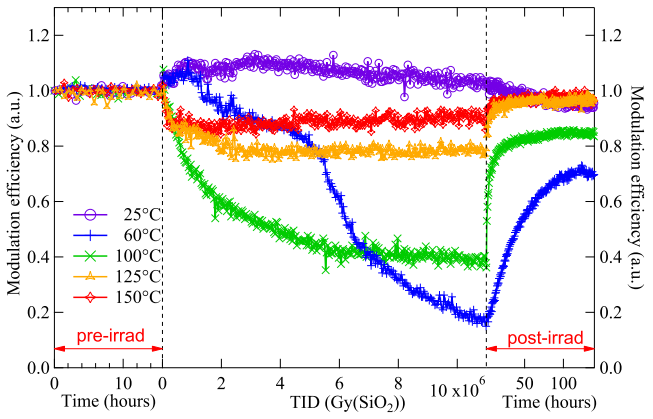

Fig. 11. Modulation efficiency of RMs of the PICv2 for the different temperatures.

C. MZM Versus RM

Finally, if the two b' modulator designs from the PICv2 are compared, the difference in their modulation efficiency can be seen in Fig. 10. It can be noticed that degradation curves have the same trend for both modulators. The MZM degrades to 40% of its initial value after 11 MGy(SiO_2). In the post-irradiation period, it keeps gradually degrading over time such that after 150 h it falls down to 35% of its initial value. Possible further degradation after this period was not recorded. The RM has slightly lower modulation efficiency during the irradiation and also much more noise in the measurement. The only difference between the two is the different kind of modulator design with different footprint dimensions.

D. RMs at Different Temperatures

In order to observe the radiation tolerance dependence on temperature, five RMs design b'' were irradiated while locally heated at temperatures in the range from 25 °C to 150 °C. The operating temperatures of the RMs were calculated according to the heater characterization carried out before the irradiation test. Based on these measurements, we applied to the heater the voltage corresponding to the desired RM temperature. The results of the first experiment are shown in Fig. 11. All mentioned devices were constantly kept at the desired temperature during the test. The device at 25 °C shows no degradation after 11 MGy(SiO_2). For the device kept at 60 °C, the degradation is significant. However, the recovery in the post-irradiation measurement is noticeable. The RM recovered from 20% of its initial efficiency up to 70% after 150 h of post-irradiation heating. The RM operated at 100 °C degraded even more quickly than the one at 60 °C, but after 11 MGy(SiO_2) it reached the stable value of 40% of its initial modulation efficiency. In the post-irradiation period, the recovery was faster than that in the case of 60 °C due to higher temperature annealing. At the end of the measurement period, the modulation efficiency of this RM was 85% of its pre-irradiation value. If we compare results at these three temperatures, the room temperature presents the best result because it does not show any degradation. However, the RM operated at room temperature is expected to degrade at a higher TID level, which is not reached in this experiment. During the post-irradiation period, RMs operated above room temperature experience recovery, while the RM at room temperature still degrades after the X-ray source was turned off. The possible explanation of this effect is the same as in Section V-B.

For higher temperatures, 125 °C and 150 °C, the degradation after 11 MGy(SiO_2) is minimal. The devices reach a stable state of 80%–90% of their initial modulation efficiency at 2 MGy(SiO_2), after which no further degradation occurs with ionizing dose. This would indicate that the recovery rate at these temperatures matches the degradation rate. For these two temperatures, the post-irradiation recovery reaches 97% of their initial performance. Running RMs above 125 °C could be an advantage with respect to lower operating temperatures thanks to the fast TID damage recovery observed during this test. Since the annealing rate is independent of the dose rate, and the degradation rate is dependent on the dose rate, a different degradation curve is expected for dose rates more similar to the LHC environment.

We have performed an accelerated test, where the 10 MGy(SiO_2) TID expected to be accumulated in ten years of operation in the innermost part of the CERN Experiments was reached in about ten days. Therefore, understanding the rate of TID damage and annealing when exposed to the dose rate present in the CERN detectors is a key point to predict the device performance across the foreseen ten years lifetime. Experiments with different dose rates are planned for the future.

VI. Conclusion

In conclusion, different SiPh modulators were tested and exposed to ionizing radiation. It was shown that the MZM with shorter w_{Dop} can withstand more TID, but not without some degradation. After 11 MGy(SiO_2) it was still operable, but with only 40% of its modulation efficiency remaining. The results also show that the RMs with higher rib doping concentration are more radiation tolerant and can withstand a TID greater than 11 MGy(SiO_2). Their transmission characteristic is flawless as it was before irradiation, demonstrating that the RMs have a great potential to be placed in the high

radiation areas of the HL-LHC experiments or in similar environments. Performance of the RMs was tested at different temperatures in the range of 25 °C–150 °C. It was shown that both low and high operating temperatures lead to lower overall degradation compared to intermediate temperatures that showed the most degradation. Significant recovery was also observed, indicating that higher temperature operation would be an effective measure to achieve ultimate radiation tolerance. It must be noted that the irradiation tests were carried out with a very high dose rate and that different results are expected with lower dose rates. This was the first experiment where this effect was observed and further studies will be carried out in the future to fully investigate it.

While previous work has shown that the TID damage is the most important factor in terms of static degradation of SiPh modulators, other effects remain to be investigated. Displacement damage is expected to occur and may become important at the high fluences estimated for the future CERN experiment environments. Single-event effects will also need to be investigated. Recent work has demonstrated the existence of optical single-event transients (OSETs) [4], a new class of effect to be studied for a wider range of structures. Further testing is being planned in order to assess the impact of the complete range of radiation effects on future SiPh test chips.

REFERENCES

[1] CERN. *High Luminosity LHC Project*. Accessed: Nov. 15, 2021. [Online]. Available: https://hilumilhc.web.cern.ch/content/hl-lhc-project

[2] S. S. E. Nasr-Storey *et al.*, "Irradiation of new optoelectronic components for HL-LHC data transmission links," *J. Instrum.*, vol. 8, no. 12, Dec. 2013, Art. no. C12040, doi: 10.1088/1748-0221/8/12/c12040.

[3] F. De Leonardis, B. Troia, C. E. Campanella, F. Prudenzano, and V. M. N. Passaro, "Modeling of radiation effects in silicon photonic devices," *IEEE Trans. Nucl. Sci.*, vol. 62, no. 5, pp. 2155–2168, Oct. 2015, doi: 10.1109/TNS.2015.2469671.

[4] G. N. Tzintzarov *et al.*, "Optical single-event transients induced in integrated silicon-photonic waveguides by two-photon absorption," *IEEE Trans. Nucl. Sci.*, vol. 68, no. 5, pp. 785–792, May 2021, doi: 10.1109/TNS.2021.3051802.

[5] A. Kraxner *et al.*, "Investigation of the influence of temperature and annealing on the radiation hardness of silicon Mach–Zehnder modulators," *IEEE Trans. Nucl. Sci.*, vol. 65, no. 8, pp. 1624–1631, Aug. 2018, doi: 10.1109/TNS.2018.2823863.

[6] G. N. Tzintzarov, S. G. Rao, and J. D. Cressler, "Integrated silicon photonics for enabling next-generation space systems," *Photonics*, vol. 8, no. 4, p. 131, Apr. 2021. [Online]. Available: https://www.mdpi.com/2304-6732/8/4/131

[7] M. Zeiler *et al.*, "Radiation damage in silicon photonic Mach–Zehnder modulators and photodiodes," *IEEE Trans. Nucl. Sci.*, vol. 64, no. 11, pp. 2794–2801, Nov. 2017. [Online]. Available: https://ieeexplore.ieee.org/document/8047293/

[8] S. S. E. Nasr-Storey *et al.*, "Neutron and X-ray irradiation of silicon based Mach–Zehnder modulators," *J. Instrum.*, vol. 10, no. 3, Mar. 2015, Art. no. C03040, doi: 10.1088/1748-0221/10/03/c03040.

[9] *IMEC*. Accessed: Nov. 15, 2021. [Online]. Available: https://europractice-ic.com/mpw-prototyping/siphotonics/imec/

[10] A. Masood *et al.*, "Fabrication and characterization of CMOS-compatible integrated tungsten heaters for thermo-optic tuning in silicon photonics devices," *Opt. Mater. Exp.*, vol. 4, no. 7, pp. 1383–1388, Jul. 2014. [Online]. Available: https://www.osapublishing.org/ome/abstract.cfm?uri=ome-4-7-1383

[11] B. S. Lee *et al.*, "On-chip thermo-optic tuning of suspended microresonators," *Opt. Exp.*, vol. 25, no. 11, pp. 12109–12120, May 2017. [Online]. Available: https://www.osapublishing.org/abstract.cfm?URI=oe-25-11-12109

[12] J. Zhang, E. Fretwurst, R. Klanner, I. Pintilie, J. Schwandt, and M. Turcato, "Investigation of X-ray induced radiation damage at the Si-SiO_2 interface of silicon sensors for the European XFEL," *J. Instrum.*, vol. 7, no. 12, Dec. 2012, Art. no. C12012, doi: 10.1088/1748-0221/7/12/c12012.

[13] H. J. Barnaby, "Total-ionizing-dose effects in modern CMOS technologies," *IEEE Trans. Nucl. Sci.*, vol. 53, no. 6, pp. 3103–3121, Dec. 2006, doi: 10.1109/TNS.2006.885952.

[14] *EP-ESE Irradiation System*. Accessed: Nov. 15, 2021. [Online]. Available: https://espace.cern.ch/project-xrayese/

[15] J. Sharma *et al.*, "Silicon photonic micro-ring modulator-based 4×112 Gb/s O-band WDM transmitter with ring photocurrent-based thermal control in 28nm CMOS," in *Proc. Symp. VLSI Circuits*, Jun. 2021, pp. 1–2, doi: 10.23919/VLSICircuits52068.2021.9492486.

[16] H. Ramon *et al.*, "Low-power 56Gb/s NRZ microring modulator driver in 28 nm FDSOI CMOS," *IEEE Photon. Technol. Lett.*, vol. 30, no. 5, pp. 467–470, Mar. 1, 2018, doi: 10.1109/LPT.2018.2799004.

[17] X. Xiao *et al.*, "High-speed, low-loss silicon Mach–Zehnder modulators with doping optimization," *Opt. Exp.*, vol. 21, no. 4, pp. 4116–4125, Feb. 2013. [Online]. Available: https://www.osapublishing.org/oe/abstract.cfm?uri=oe-21-4-4116

[18] M. Zeiler *et al.*, "Radiation hardness evaluation and phase shift enhancement through ionizing radiation in silicon Mach–Zehnder modulators," in *Proc. 16th Eur. Conf. Radiat. Effects Compon. Syst. (RADECS)*, Sep. 2016, pp. 163–166, doi: 10.1109/RADECS.2016.8093130.

[19] M. Zeiler *et al.*, "Design of Si-photonic structures to evaluate their radiation hardness dependence on design parameters," *J. Instrum.*, vol. 11, no. 1, Jan. 2016, Art. no. C01040. [Online]. Available: https://iopscience.iop.org/article/10.1088/1748-0221/11/01/C01040